NANO LETTERS

Letter

pubs.acs.org/NanoLett

Suppressed Blinking and Auger Recombination in Near-Infrared Type-II InP/CdS Nanocrystal Quantum Dots

Allison M. Dennis,[†] Benjamin D. Mangum,[†] Andrei Piryatinski,[‡] Young-Shin Park,[†] Daniel C. Hannah,[∥] Joanna L. Casson,[§] Darrick J. Williams,[†] Richard D. Schaller,[∥,⊥] Han Htoon,[†] and Jennifer A. Hollingsworth*,[†]

[†]Materials Physics & Applications Division: Center for Integrated Nanotechnologies, Los Alamos National Laboratory, Los Alamos, New Mexico 87545, United States

[‡]Theoretical Division, Los Alamos National Laboratory, Los Alamos, New Mexico 87545, United States

[§]Chemistry Division, Los Alamos National Laboratory, Los Alamos, New Mexico 87545, United States

[∥]Department of Chemistry, Northwestern University, Evanston, Illinois 60208, United States

[⊥]Center for Nanoscale Materials, Argonne National Laboratory, Argonne, Illinois 60439, United States

Supporting Information

ABSTRACT: Nonblinking excitonic emission from near-infrared and type-II nanocrystal quantum dots (NQDs) is reported for the first time. To realize this unusual degree of stability at the single-dot level, novel InP/CdS core/shell NQDs were synthesized for a range of shell thicknesses (~1−11 monolayers of CdS). Ensemble spectroscopy measurements (photoluminescence peak position and radiative lifetimes) and electronic structure calculations established the transition from type-I to type-II band alignment in these heterostructured NQDs. More significantly, single-NQD studies revealed clear evidence for blinking suppression that was not strongly shell-thickness dependent, while photobleaching and biexciton lifetimes trended explicitly with extent of shelling. Specifically, very long biexciton lifetimes—up to >7 ns—were obtained for the thickest-shell structures, indicating dramatic suppression of nonradiative Auger recombination. This new system demonstrates that electronic structure and shell thickness can be employed together to effect control over key single-dot and ensemble NQD photophysical properties.

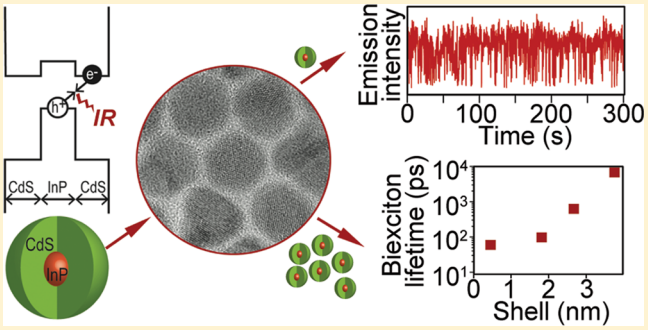

KEYWORDS: *Fluorescence blinking suppression, core/shell heterostructure, near-infrared, type-II nanocrystal quantum dot, biexciton lifetime, Auger recombination*

Fluorescence intermittency, or blinking, is exhibited by a number of fluorophores, including molecular dyes,[1] fluorescent proteins,[2] and nanocrystal quantum dots (NQDs).[3,4] Blinking behavior in NQDs has most commonly been attributed to the coupling of random charging/discharging events with activation of efficient nonradiative Auger recombination (AR) in charged or ionized NQDs.[5] Attempts to suppress fluorescence intermittency in this class of emitter have often entailed addressing the charging portion of the blinking problem through supplementation with external reducing or electron-donating species (e.g., β-mercaptoethanol, propyl gallate) that electronically passivate surface trap states and suppress pathways for photoinduced charge formation[6−8] or the use of charge-accepting species (e.g., TiO_2 nanoparticles) to provide enhanced routes for "de-trapping" and reneutralization.[9] In contrast, modification of the NQD geometry or internal structure alters intrinsic AR, such as when AR is suppressed in elongated (larger volume) nanorods, where exciton−exciton coupling is reduced,[10] or in type-II or quasi-type-II heterostructures (carriers spatially separated), where electron−hole overlap is reduced and even repulsive Coulombic interactions can develop.[11] Alloying of the core/shell interface can also suppress AR by inducing a smoothing of the confinement potential.[5,12]

To date, explicit experimental correlation of AR suppression with room-temperature blinking suppression has been limited to an alloyed CdZnSe/ZnSe NQD system[12] and a quasi-type-II, thick-shell CdSe/CdS system,[13−17] where the latter (so-called g-NQDs[13]) likely benefits from both suppressed charging (due to the thick, protective shell limiting ionization processes and/or possibly carrier trapping) and suppressed AR (due to a combination of size, carrier-separation, and possibly interface effects[17]). The ability to simultaneously suppress blinking and

Received: July 2, 2012
Revised: September 7, 2012
Published: September 14, 2012

nonradiative AR has important implications for a range of applications from single-particle tracking in the biosciences[14] to low-threshold multicolor lasing[17] and efficient multiexciton emission and extraction.[18] Here, we move beyond the limited examples of CdSe-based core/shell engineering to show that judicious NQD heterostructuring can afford significantly suppressed blinking and AR in InP-based NQDs, demonstrating the approach as a general method for effecting control over key NQD light-emission properties. Specifically, we show that a new InP/CdS NQD system exhibits both suppressed blinking and AR, similarly to their thick-shell CdSe/CdS g-NQD counterparts. However, unlike the earlier system, blinking suppression is not strictly confined to thick shells. Furthermore, InP/CdS NQDs are distinguished by their fully type-II bandgap alignment, which affords complete spatial separation of excited-state carriers and transitions the room-temperature nonblinking excitonic emission for the first time into the near-infrared. Significantly, room-temperature blinking behavior for a fully type-II system has also not been previously demonstrated, as attempts have been thwarted by extreme sensitivity to photobleaching and a low signal-to-noise ratio at the single-dot level.[19]

In this work, we address the effects of both type-II electronic structure and shell thickness. To this end, we developed the novel InP/CdS core/shell NQD. Consideration of the alignment of electronic states for the bulk InP-CdS interface reveals that InP/CdS NQDs should afford a fully charge-separated (type-II) state, where electrons reside in the CdS shell and holes are confined to the InP core (Figure 1a).

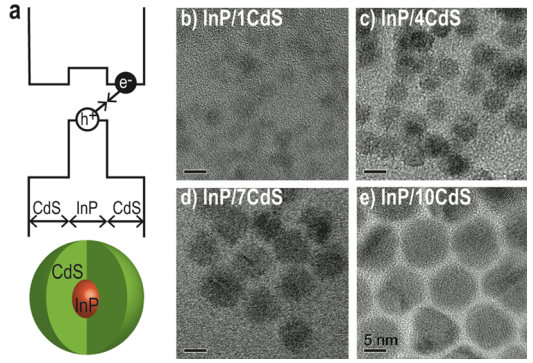

Figure 1. InP/CdS core/shell NQDs. (a) Schematic of the InP/CdS core/shell structure and the relative bulk bandgap alignment of the core and shell materials. Localization of the excited electron in the CdS shell and the resulting hole in the InP core is indicative of type-II bandgap structure. (b–e) TEM images of InP/CdS core/shell nanocrystals after 1, 4, 7, and 10 successive shell depositions, respectively. The scale bar for all four images is 5 nm.

Furthermore, our core/shell synthesis approach allows us to fabricate CdS-overcoated InP NQDs with shell thicknesses ranging from 1 to >11 monolayers (MLs). Similar to our CdSe/CdS g-NQD synthesis, the CdS shell is deposited monolayer-by-monolayer onto the InP cores through a successive ionic layer adsorption and reaction (SILAR) method (see the Supporting Information).[13,14,20] However, compared to CdSe, InP cores are significantly more susceptible to surface oxidation and particle etching,[21] the former requiring unusual care in applying air-free procedures prior to shell growth and the latter preventing use of high growth temperatures combined with acidic or basic ligands.[22] It is likely for these reasons that relatively fewer successful high-temperature, SILAR-based preparations of core/shell NQDs with InP cores have been reported.[23] To render InP NQDs amenable to thick-shell CdS shell growth, we devised a method whereby the initial shell monolayer is applied using lower, nonideal shell-growth temperatures and serves as a "protective" layer for subsequent shell additions that employ conditions optimized for higher quality shell growth.

Overall, InP cores (2.46 nm diameter) were exposed to 10 successive cation/anion addition cycles. Analysis of transmission electron microscopy (TEM) images (Figure 1b–e, Table 1) reveals increasing shell thickness with each shell addition cycle, with slightly more than one monolayer added per iteration. For example, one shell addition cycle ("InP/1CdS") affords approximately 1.6 monolayers of CdS, while 10 shell addition cycles ("InP/10CdS") yields 11.4 monolayers of CdS shell. TEM analysis also demonstrates the reasonably uniform particle size and morphology achieved for this system, with deviations in diameter size of ~10% (Table 1). Small-angle X-ray diffraction (XRD) of thick-shell InP/CdS NQDs, which comprise predominantly CdS (>98% CdS by volume for InP/10CdS), reveals that CdS retains its thermodynamic hexagonal (wurtzite) crystal structure even though it has been applied to cubic (zinc-blende) InP NQDs (Figure S1, Supporting Information). Despite the inequivalencies in crystal structure and no compositional commonalities between the core and the shell materials, the InP/CdS NQDs benefit from a small lattice mismatch (<1%) and exhibit remarkably regular shapes, characterized by hexagonal faceting as shell thickness is increased (Figure 1b–e). The shell quality stands in contrast with some previously reported type-II systems[24,25] but is similar to our CdSe/CdS g-NQD system.[13] Based on these similarities in *physical* structure with the prototype g-NQD system, the InP/CdS NQDs allow direct assessments of blinking and AR suppression in terms of shell-thickness effects.

With respect to electronic structure, we find clear spectral and dynamic signatures of a type-II heterojunction. In type-II systems, the bandgap energy derives from a spatially *indirect* transition,[25,29] or charge-transfer state,[30] that involves electron–hole recombination across the core–shell interface, as the carriers are spatially confined to different regions of the heterostructure (Figure 1a). Thus, the bandgap can be smaller than that achievable by either the emitting core or the shell material alone, and exciton lifetimes are typically long.[24,31] For InP/CdS, we find that photoluminescence (PL) and bandgap energies indeed progress toward lower energies as CdS shells are added to InP (Table 1, Figure 2a,b), and PL lifetimes increase (Table 1, Figure 2c). Spectral red-shifting is clearly evident with the addition of the first several shell monolayers, after which changes in PL energy as a function of shell thickness are less substantial (Table 1, Figure 2b). Specifically, the addition of only three CdS monolayers (InP/2CdS) results in a 1.46 eV core/shell emission energy that is >600 meV red-shifted from the ~2.1 eV starting InP core value (necessarily estimated here from the InP core absorption 1S peak, as core-only emission is negligible). The final emission energy reached by thicker shell InP/CdS NQDs (~1.25 eV) is less than the bulk bandgap of InP (1.34 eV). For all shell thicknesses, core/shell bandgap energies are smaller ("redder") than the bandgap energies for equivalently sized InP NQDs (Figure 2b), consistent with the formation of a type-II electronic structure at very early stages of shell growth. This conclusion is supported by theoretical modeling of carrier localization

dx.doi.org/10.1021/nl302453x | *Nano Lett.* 2012, 12, 5545–5551

Table 1. Summary of InP/CdS NQD Properties

no. of CdS shell-addition cycles	diameter[a] (nm)	shell thickness (nm)	no. of shell MLs from TEM analysis	PL peak position (nm/eV)	PL fwhm (nm/eV)	average PL lifetime, τ_x (ns)	biexciton lifetime, τ_{xx} (ps)
InP core	2.46	n/a	n/a	~600/2.1[b]	n/a	80−150[c]	n/a
InP/1CdS	3.52 ± 0.38 (11%)	0.53	1.6	696/1.78	124/0.32	190	58 ± 12
InP/2CdS	4.56 ± 0.49 (11%)	1.05	3.1	849/1.46	476/0.38	327	n/a
InP/3CdS	5.40 ± 0.52 (10%)	1.47	4.4	904/1.37	483/0.34	349	n/a
InP/4CdS	6.26 ± 0.65 (10%)	1.90	5.6	937/1.32	211/0.29	435	99 ± 5
InP/7CdS	7.97 ± 0.84 (10%)	2.76	8.2	982/1.26	220/0.28	575	612 ± 49
InP/10CdS	10.13 ± 0.90 (9%)	3.84	11.4	1000/1.24	229/0.28	702	7212 ± 1073

[a]InP core diameter determined from 1S peak position.[26] InP/CdS core/shell diameter determined from TEM image analysis. Error represents standard deviation of 157−485 measured dots. [b]InP cores are nonemissive, so PL peak position derived from 1S peak position (544 nm/2.28 eV) plus an estimated Stokes shift. [c]Lifetime values for InP from the literature.[27,28] See Supporting Information, Table S1.

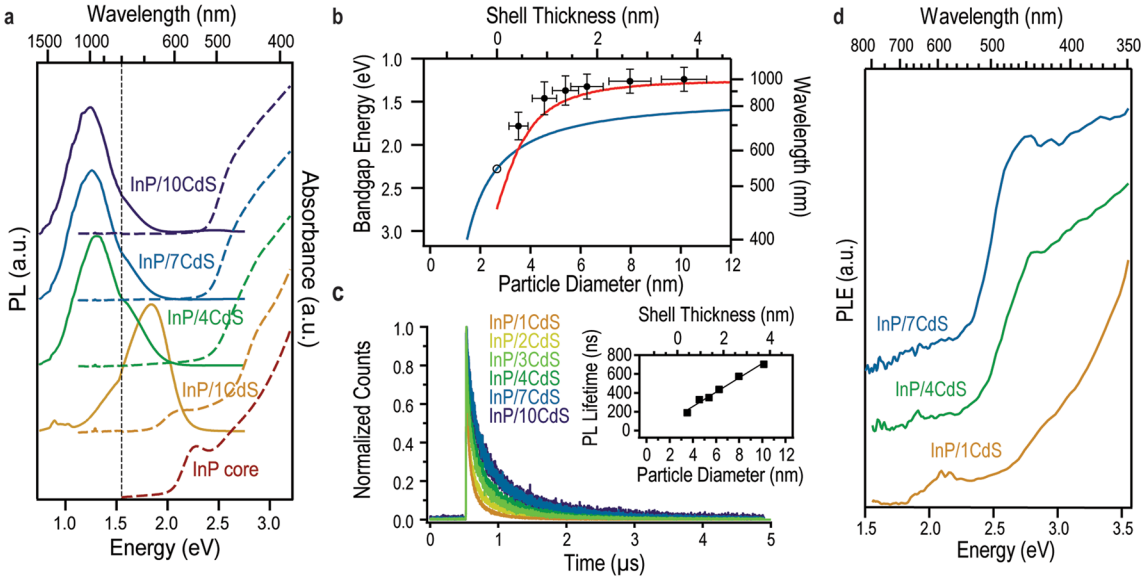

Figure 2. Ensemble spectroscopy. (a) Absorption (dashed lines) and photoluminescence (PL) (solid lines) spectra of the InP core and InP/CdS core/shell structures (excitation at 405 nm). The dashed line at 800 nm indicates where PL detectors were switched. Shoulders in the PL peaks in this region are artifacts of using two different detectors. (b) Bandgap energy vs particle size. The InP core bandgap energy (data point without error bars) was determined by the 1S peak in the absorbance measurement, while the InP/CdS core/shell bandgap energies (remaining points) represent PL energies. One core size is depicted with multiple shell thicknesses. The blue line represents the bandgap energy expected for an InP NQD at various sizes. The red line depicts our predicted bandgap energy for a specific core/shell size combination (i.e., core size and shell thickness). Error bars in the x and y represent the standard deviation of the particle size and fwhm of the PL peak, respectively. (c) PL lifetime measurements. Inset: plot of average lifetime vs shell thickness. (d) Photoluminescence excitation spectra (PLE) of several InP/CdS structures. Emission set at 650, 875, and 900 nm for the InP/1CdS, InP/4CdS, and InP/7CdS samples, respectively.

behavior in InP/CdS NQDs using the effective mass approximation (Supporting Information), which affords a similar trend in bandgap changes as a function of shell thickness (Figure 2b, red trace). In contrast to energy shifting trends, average PL lifetimes increase roughly linearly with shell thickness, reaching an ~7-fold enhancement compared to InP cores at the thickest shells (11.4 MLs) (Tables 1 and S1, Figure 2c). Here, ensemble PL lifetimes of drop-cast NQD films were measured using time-correlated single-photon counting (TCSPC) and a triexponential fit to the histogram of photon arrival times. Average lifetime values were calculated using the various fit components as described in the Supporting Information.

Absorption spectra also reveal the transition to type-II behavior. Here, the well-defined 1S absorption peak of the starting InP cores is broadened and red-shifted by initial shell addition, consistent with previous accounts of type-II NQD absorption trends.[24] InP/CdS NQD absorption is subsequently dominated by the thick CdS shell at wavelengths <520 nm, resulting in *blue-shifting* of the absorption onset and a larger effective Stokes shift (separation between emission and absorption), like CdSe/CdS g-NQDs but unlike previously reported type-II NQDs. Significantly, we find that photoluminescence excitation (PLE) spectra follow similar trends as the absorption spectra (Figure 2d), suggesting that energy relaxation from a shell-derived excited state to the indirect or

dx.doi.org/10.1021/nl302453x | *Nano Lett.* 2012, 12, 5545−5551

charge-transfer emitting state is efficient and dominates emission.

To determine how shell thickness and a type-II electronic structure influence charging and AR-mediated processes, we attempted to assess single-dot-level blinking behavior, as well as photostability and biexciton lifetimes. Notably, room-temperature blinking studies on fully type-II core/shell NQDs have not been reported to date. Though such studies are now well-known in the case of quasi-type-II CdSe/CdS[13−15] and presumed quasi-type-II CdTe/CdTe$_x$Se$_y$/CdSe NQDs,[19] photobleaching under single-dot excitation conditions has prevented such analyses on type-II systems.[19] Perhaps more strikingly, single-NQD spectroscopy for any type of NQD emitting in the near-infrared has thus far been limited to a single report. In that case, even nominally brighter type-I infrared-emitting NQDs proved difficult to assess by this method, requiring use of highly specialized single-photon detectors to surmount materials issues of instability and relatively long emission lifetimes.[32] This omission to date stands in stark contrast to self-assembled epitaxial quantum dot reports that have benefitted from the relative photostability and shorter radiative lifetimes of these noncolloidal systems.[32]

Unlike prior efforts, standard sample preparation and single-photon detection methods proved adequate, though not ideal (see below), for obtaining intensity-versus-time traces at the single-NQD level. Specifically, freshly prepared, ultradilute solutions were spread onto glass slides, and the resulting dispersion of single InP/CdS NQDs were interrogated using a continuous wave (CW) laser at 405 nm. Photons were collected on an avalanche photodiode (APD) detector in single-photon-counting mode, and the PL intensity time trace was analyzed using a 20 ms bin time. We were able to obtain single-NQD data for the full range of shell thicknesses.

Interestingly, with respect to blinking behavior, a simple shell-thickness dependence was *not* observed (Figure 3), in contrast with the quasi-type-II CdSe/CdS system.[14] For example, some relatively thin-shell InP/1CdS and InP/4CdS NQDs exhibited conventional blinking behavior, while others exhibited blinking suppression (Figure 3a), with ∼15−25% of the dots demonstrating on-time fractions of >80% of the observation time (5 min). Notably, conventional blinking behavior (e.g., that typical of CdSe/ZnS NQDs) is characterized by 0% of a NQD population possessing on-time fractions >80%.[14] Blinking suppression does improve as shell thickness is increased to 3.84 nm (InP/10CdS), though not as dramatically as observed for CdSe/CdS g-NQD shell-thickness trends. That said, >60% of the InP/10CdS NQDs are on >80% of the observation time, and several dots are observed to be essentially nonblinking, that is, on-time fractions ∼95% (Figure 3a, InP/10CdS "dot indices" 2, 9, 10, and 11). Given the difficulties of performing single-dot-level measurements in the near-infrared,[32] our "blinking" data set is relatively limited (total dot numbers in the tens compared to hundreds typical for visible-emitting NQDs). Thus, while it is clear that blinking is suppressed in the InP/CdS system, the precise shell-thickness dependence and nonblinking dot fractions remain to be determined as measurement techniques improve.

We also studied photobleaching behavior for thin (InP/1CdS and InP/4CdS) and thick-shell (InP/10CdS) samples over a 3 h period with continuous laser excitation. Here, shell-thickness dependency is more evident (Figure 3c). InP/1CdS NQDs essentially completely photobleach over the course of the experiment, while ∼20% of InP/4CdS NQDs continue to emit

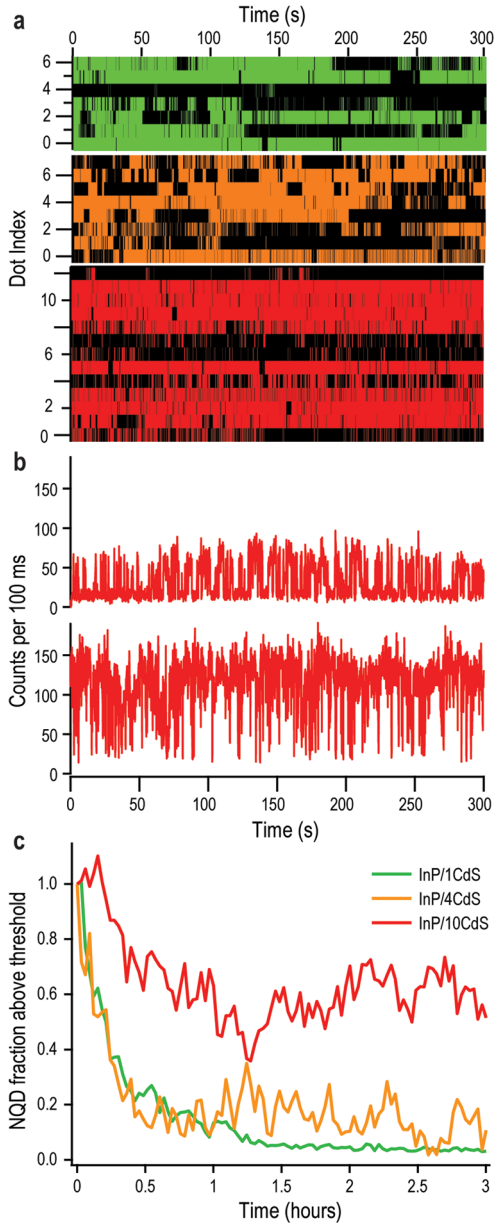

Figure 3. Blinking and photobleaching. (a) Summary of blinking behavior for multiple individual NQDs for several shell thicknesses. Each dot index represents the blinking behavior of one dot. Black regions in each image represent times when the dot is in the "off" state. Colored regions correspond to "on" states. Green, orange, and red traces represent single dot data from InP/1CdS, InP/4CdS, and InP/10CdS, respectively. (b) Representative intensity trajectories of single NQDs (both InP/10CdS). The top and bottom traces correspond to dot indices 4 and 10 in the top panel, respectively. (c) Relative photobleaching from each sample over time. NQDs dropcast and imaged under widefield laser excitation (405 nm) using a CCD with 1 s integration time for three hours. The number of dots having a PL intensity above a threshold value was tabulated for each frame. The fraction of dots meeting this criteria (relative to the number of dots present at t = 0) is plotted as a function of time.

for the duration of the experiment. In contrast, ∼60% of InP/10CdS NQDs do not photobleach. In all cases, the observed declines in PL occur during the first ∼30 min of the experiment, suggesting that NQDs that are inclined to photobleach do so in a manner that is consistent with that observed for conventional core/shell NQDs for which the

dx.doi.org/10.1021/nl302453x | *Nano Lett.* 2012, 12, 5545−5551

photobleaching half-life ($t_{1/2}$) is ~15 min.[13,14] The remaining nonphotobleaching dot population (~20% of InP/4CdS and ~60% of InP/10CdS) is photostable, exhibiting no further decline over the 3 h observation time. Thus, thicker CdS shells promote improved photostability, relevant for a range of potential applications from single-photon light sources to single-molecule tracking in biology.

In an attempt to understand the observed blinking suppression in terms of contributions from different aspects of the core/shell structure, especially shell thickness and electronic structure, we consider further the underlying processes that can lead to blinking in NQDs. Specifically, fluorescence intermittency in NQDs was recently shown to result from one of two mechanisms: (1) the "conventional" charging model that describes blinked-off events as resulting from efficient nonradiative AR in charged NQDs and (2) hot-electron capture to surface trap-states that short circuits radiative electron–hole recombination but does not invoke NQD-charging or AR processes.[33] The addition of a high-quality thick shell might be expected to suppress charging and hot-electron-capture pathways by minimizing carrier tunneling and core/surface-state interactions, respectively, thereby suppressing both blinking mechanisms. This seems a reasonable implication of applying thicker and thicker CdS shells to InP. However, our observations of this system show that blinking suppression is possible even for thin CdS shells, for which neither suppressed charging nor suppressed surface-state trapping should be expected. In this case, reduced AR efficiency is possibly a significant factor in the observed blinking-suppressed behavior. Indeed, AR efficiencies are in general reduced in type-II core/shell NQDs compared to type-I NQDs due to lessened electron–hole overlap and/or exciton–exciton repulsion.[24]

To confirm AR suppression in the new type-II InP/CdS NQDs and to establish any shell-thickness dependencies, we obtained pump-intensity-dependent PL decay time traces for multiple shell thicknesses and extracted biexciton lifetimes (τ_{xx}). Longer biexciton lifetimes indicate reduced AR efficiencies.[17] We find that biexciton lifetimes exhibit a dependence on shell thickness (Figure 4) and are substantially longer for the thickest-shell sample (by a factor of ~125 for 10CdS vs 1CdS). Significantly, however, although this shell-dependent lengthening of the biexciton lifetime is dramatic, τ_{xx} remains short compared to τ_x (InP/10CdS: $\tau_x/\tau_{xx} = 97.5$; Table 1). According to established theories of radiative decay in NQDs, *radiative biexciton* lifetimes should be reduced compared to *radiative exciton* lifetimes by only a factor of 2–4.[27] The observed deviation of InP/CdS τ_{xx} values from ideal radiative biexciton lifetimes (i.e., from $\tau_x/\tau_{xx} \approx 2 - 4$) results from contributions from nonradiative processes, likely primarily AR.[17] In this way, the ratio between single and biexciton lifetimes gives a measure of the relative strength of AR. It is then apparent that although nonradiative AR is greatly diminished in this system with increasing shell thickness (e.g., comparing InP/10CdS to InP/1CdS τ_x/τ_{xx}: 97.5 vs 3276, respectively), AR is still not zero and is capable of contributing to less-than-optimal biexciton efficiencies. For this reason, we cannot conclusively state that the observed AR suppression is sufficient to explain the InP/CdS blinking suppression based on an AR model, and, thus, it remains to be determined what blinking pathways are important in this unusual system. Nevertheless, the remarkable enhancement in biexciton lifetime with increasing shell thickness has important implications for

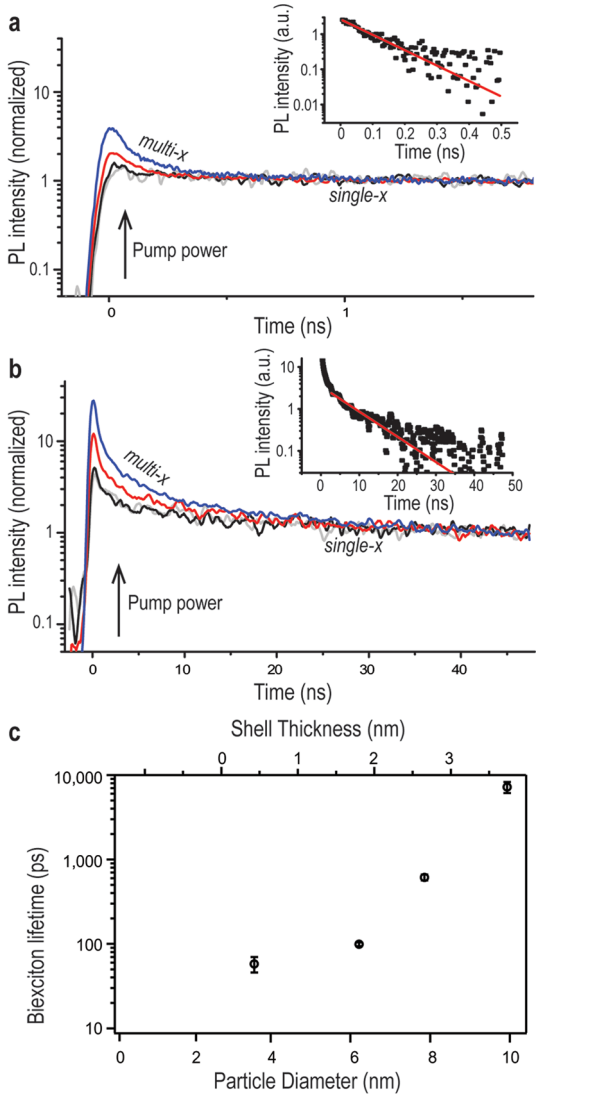

Figure 4. Biexciton lifetimes. (a) Spectrally integrated transient-PL measurements for a 5.2 nm diameter InP/CdS core/shell sample (InP/4CdS) in dilute toluene solution at different 3.1 eV pump fluences (1–170 μJ/cm^2). Traces normalized at 1.8 ns show that all multiexciton signals have decayed within less than 500 ps. The inset shows the extracted multiexciton decay component as well as a single exponential fit (red line) with a 99 ± 4 ps biexciton decay. (b) For an 8.3 nm diameter core/shell sample (InP/10CdS), pump-intensity-dependent transient-PL measurements normalized at 48 ns do not fully converge until ~30 ns, indicating long-lived multiexcitons. A single exponential fit (red line) to the extracted multiexciton component (shown in the inset) reveals long-lived multiexcitons. (c) Fitted biexciton lifetimes extracted from time-resolved PL data show a large lifetime increase as a function of shell thickness and total particle diameter.

applications of this new g-NQD system in optical amplification and lasing, where stimulated emission most directly competes with Auger relaxation, and single-exciton recombination processes are less relevant.[34]

From the perspective of intentional design of functional nanoscale structures and interfaces, we have shown that both the physical structure (thick shell) and the electronic structure (charge-separated excited state or type-II alignment of energy bands) are important design parameters for realizing unusual and practical photophysical properties. This novel example of

dx.doi.org/10.1021/nl302453x | Nano Lett. 2012, 12, 5545–5551

thick-shell heterostructuring demonstrates that photostability at both the single-NQD and the ensemble levels, as well as intrinsic NQD properties such as AR, can be tuned by considering both physical and electronic-structure effects. These new InP/CdS near-infrared emitters—characterized by significant room-temperature photostability and blinking- and AR-suppressed behavior—open immediate opportunities from advanced bioimaging/single-particle tracking to low-threshold near-IR lasing. They have also permitted for the first time analysis by standard single-NQD spectroscopy methods of near-infrared emission at the single-particle level.

■ ASSOCIATED CONTENT

Ⓢ Supporting Information

Experimental methods, theoretical modeling details, XRD data, and PL lifetime measurement fit parameters. This material is available free of charge via the Internet at http://pubs.acs.org.

■ AUTHOR INFORMATION

Corresponding Author

*E-mail: jenn@lanl.gov.

Notes

The authors declare no competing financial interest.

■ ACKNOWLEDGMENTS

A.P. and J.C. acknowledge support by the Los Alamos National Laboratory Directed Research and Development (LDRD) Program. A.M.D., B.D.M., D.C.H. and H.H. acknowledge a Single Investigator Small Group Research Grant (2009LANL1096), Office of Basic Energy Sciences (OBES), Office of Science (OS), U.S. Department of Energy (DOE). Y.-S.P. and D.W. are supported by the Center for Integrated Nanotechnologies (CINT). J.A.H. is supported, in part, by NIH-NIGMS Grant 1R01GM084702-01. This work was performed, in part, at the Center for Integrated Nanotechnologies, a U.S. Department of Energy, Office of Basic Energy Sciences user facility. Los Alamos National Laboratory, an affirmative action equal opportunity employer, is operated by Los Alamos National Security, LLC, for the National Nuclear Security Administration of the U.S. Department of Energy under contract DE-AC52-06NA25396. Use of the Center for Nanoscale Materials (R.D.S. and D.C.H.) was supported by the U. S. Department of Energy, Office of Science, Office of Basic Energy Sciences, under Contract No. DE-AC02-06CH11357.

■ REFERENCES

(1) Hoogenboom, J. P.; Hernando, J.; van Dijk, E. M. H. R.; van Hulst, N. F.; Garcia-Parajo, M. F. Power-law blinking in the fluorescence of single organic molecules. *ChemPhysChem* **2007**, *8*, 823−833.

(2) Dickson, R. M.; Cubitt, A. B.; Tsien, R. Y.; Moerner, W. E. On/off blinking and switching behaviour of single molecules of green fluorescent protein. *Nature* **1997**, *388*, 355−358.

(3) Kuno, M.; Fromm, D. P.; Hamann, H. F.; Gallagher, A.; Nesbitt, D. J. Nonexponential "blinking" kinetics of single CdSe quantum dots: A universal power law behavior. *J. Chem. Phys.* **2000**, *112*, 3117−3120.

(4) Kuno, M.; Fromm, D. P.; Gallagher, A.; Nesbitt, D. J.; Micic, O. I.; Nozik, A. J. Fluorescence intermittency in single InP quantum dots. *Nano Lett.* **2001**, *1*, 557−564.

(5) Cragg, G. E.; Efros, A. L. Suppression of Auger Processes in Confined Structures. *Nano Lett.* **2010**, *10*, 313−317.

(6) Hohng, S.; Ha, T. Near-complete suppression of quantum dot blinking in ambient conditions. *J. Am. Chem. Soc.* **2004**, *126*, 1324−1325.

(7) Fomenko, V.; Nesbitt, D. J. Solution control of radiative and nonradiative lifetimes: A novel contribution to quantum dot blinking suppression. *Nano Lett.* **2008**, *8*, 287−293.

(8) Jeong, S.; Achermann, M.; Nanda, J.; Ivanov, S.; Klimov, V. I.; Hollingsworth, J. A. Effect of the thiol-thiolate equilibrium on the photophysical properties of aqueous CdSe/ZnS nanocrystal quantum dots. *J. Am. Chem. Soc.* **2005**, *127*, 10126−10127.

(9) Hamada, M.; Nakanishi, S.; Itoh, T.; Ishikawa, M.; Biju, V. Blinking Suppression in CdSe/ZnS Single Quantum Dots by TiO_2 Nanoparticles. *ACS Nano* **2010**, *4*, 4445−4454.

(10) Htoon, H.; Hollingsworth, J. A.; Dickerson, R.; Klimov, V. I. Effect of zero- to one-dimensional transformation on multiparticle Auger recombination in semiconductor quantum rods. *Phys. Rev. Lett.* **2003**, *91*.

(11) Nanda, J.; Ivanov, S. A.; Achermann, M.; Bezel, I.; Piryatinski, A.; Klimov, V. I. Light amplification in the single-exciton regime using exciton-exciton repulsion in type-II nanocrystal quantum dots. *J. Phys. Chem. C* **2007**, *111*, 15382−15390.

(12) Wang, X. Y.; Ren, X. F.; Kahen, K.; Hahn, M. A.; Rajeswaran, M.; Maccagnano-Zacher, S.; Silcox, J.; Cragg, G. E.; Efros, A. L.; Krauss, T. D. Non-blinking semiconductor nanocrystals. *Nature* **2009**, *459*, 686−689.

(13) Chen, Y.; Vela, J.; Htoon, H.; Casson, J. L.; Werder, D. J.; Bussian, D. A.; Klimov, V. I.; Hollingsworth, J. A. "Giant" multishell CdSe nanocrystal quantum dots with suppressed blinking. *J. Am. Chem. Soc.* **2008**, *130*, 5026−5027.

(14) Vela, J.; Htoon, H.; Chen, Y.; Park, Y.-S.; Ghosh, Y.; Goodwin, P. M.; Werner, J. H.; Wells, N. P.; Casson, J. L.; Hollingsworth, J. A. Effect of shell thickness and composition on blinking suppression and the blinking mechanism in "giant" CdSe/CdS nanocrystal quantum dots. *J. Biophotonics* **2010**, *3*, 706−717.

(15) Mahler, B.; Spinicelli, P.; Buil, S.; Quelin, X.; Hermier, J. P.; Dubertret, B. Towards non-blinking colloidal quantum dots. *Nat. Mater.* **2008**, *7*, 659−664.

(16) Spinicelli, P.; Buil, S.; Quelin, X.; Mahler, B.; Dubertret, B.; Hermier, J. P. Bright and Grey States in CdSe-CdS Nanocrystals Exhibiting Strongly Reduced Blinking. *Phys. Rev. Lett.* **2009**, *102*.

(17) García-Santamaría, F.; Chen, Y.; Vela, J.; Schaller, R. D.; Hollingsworth, J. A.; Klimov, V. I. Suppressed Auger Recombination in "Giant" Nanocrystals Boosts Optical Gain Performance. *Nano Lett.* **2009**, *9*, 3482−3488.

(18) Htoon, H.; Malko, A. V.; Bussian, D.; Vela, J.; Chen, Y.; Hollingsworth, J. A.; Klimov, V. I. Highly Emissive Multiexcitons in Steady-State Photoluminescence of Individual "Giant" CdSe/CdS Core/Shell Nanocrystals. *Nano Lett.* **2010**, *10*, 2401−2407.

(19) Chon, B.; Bang, J.; Park, J.; Jeong, C.; Choi, J. H.; Lee, J. B.; Joo, T.; Kim, S. Unique Temperature Dependence and Blinking Behavior of CdTe/CdSe (Core/Shell) Type-II Quantum Dots. *J. Phys. Chem. C* **2011**, *115*, 436−442.

(20) Li, J. J.; Wang, Y. A.; Guo, W. Z.; Keay, J. C.; Mishima, T. D.; Johnson, M. B.; Peng, X. G. Large-scale synthesis of nearly monodisperse CdSe/CdS core/shell nanocrystals using air-stable reagents via successive ion layer adsorption and reaction. *J. Am. Chem. Soc.* **2003**, *125*, 12567−12575.

(21) Jasinski, J.; Leppert, V. J.; Lam, S. T.; Gibson, G. A.; Nauka, K.; Yang, C. C.; Zhou, Z. L. Rapid oxidation of InP nanoparticles in air. *Solid State Commun.* **2007**, *141*, 624−627.

(22) Ryu, E.; Kim, S.; Jang, E.; Jun, S.; Jang, H.; Kim, B.; Kim, S. W. Step-Wise Synthesis of InP/ZnS Core-Shell Quantum Dots and the Role of Zinc Acetate. *Chem. Mater.* **2009**, *21*, 573−575.

(23) Xie, R. G.; Peng, X. G. Synthesis of Cu-Doped InP Nanocrystals (d-dots) with ZnSe Diffusion Barrier as Efficient and Color-Tunable NIR Emitters. *J. Am. Chem. Soc.* **2009**, *131*, 10645−10651.

(24) Lo, S. S.; Mirkovic, T.; Chuang, C. H.; Burda, C.; Scholes, G. D. Emergent Properties Resulting from Type-II Band Alignment in Semiconductor Nanoheterostructures. *Adv. Mater.* **2011**, *23*, 180−197.

(25) Piryatinski, A.; Ivanov, S. A.; Tretiak, S.; Klimov, V. I. Effect of quantum and dielectric confinement on the exciton-exciton interaction energy in type II core/shell semiconductor nanocrystals. *Nano Lett.* **2007**, *7*, 108−115.
(26) Xie, R. G.; Li, Z.; Peng, X. G. Nucleation Kinetics vs Chemical Kinetics in the Initial Formation of Semiconductor Nanocrystals. *J. Am. Chem. Soc.* **2009**, *131*, 15457−15466.
(27) Micic, O. I.; Cheong, H. M.; Fu, H.; Zunger, A.; Sprague, J. R.; Mascarenhas, A.; Nozik, A. J. Size-dependent spectroscopy of InP quantum dots. *J. Phys. Chem. B* **1997**, *101*, 4904−4912.
(28) Li, C.; Ando, M.; Enomoto, H.; Murase, N. Highly Luminescent Water-Soluble InP/ZnS Nanocrystals Prepared via Reactive Phase Transfer and Photochemical Processing. *J. Phys. Chem. C* **2008**, *112*, 20190−20199.
(29) Ivanov, S. A.; Piryatinski, A.; Nanda, J.; Tretiak, S.; Zavadil, K. R.; Wallace, W. O.; Werder, D.; Klimov, V. I. Type-II core/shell CdS/ZnSe nanocrystals: Synthesis, electronic structures, and spectroscopic properties. *J. Am. Chem. Soc.* **2007**, *129*, 11708−11719.
(30) Chuang, C. H.; Doane, T. L.; Lo, S. S.; Scholes, G. D.; Burda, C. Measuring Electron and Hole Transfer in Core/Shell Nanoheterostructures. *ACS Nano* **2011**, *5*, 6016−6024.
(31) Kim, S.; Fisher, B.; Eisler, H. J.; Bawendi, M. Type-II quantum dots: CdTe/CdSe(core/shell) and CdSe/ZinTe(core/shell) heterostructures. *J. Am. Chem. Soc.* **2003**, *125*, 11466−11467.
(32) Correa, R. E.; Dauler, E. A.; Nair, G.; Pan, S. H.; Rosenberg, D.; Kerman, A. J.; Molnar, R. J.; Hu, X.; Marsili, F.; Anant, V.; Berggren, K. K.; Bawendi, M. G. Single Photon Counting from Individual Nanocrystals in the Infrared. *Nano Lett.* **2012**, *12*, 2953−2958.
(33) Galland, C.; Ghosh, Y.; Steinbruck, A.; Sykora, M.; Hollingsworth, J. A.; Klimov, V. I.; Htoon, H. Two types of luminescence blinking revealed by spectroelectrochemistry of single quantum dots. *Nature* **2011**, *479*, 203−207.
(34) Klimov, V. I.; Mikhailovsky, A. A.; Xu, S.; Malko, A.; Hollingsworth, J. A.; Leatherdale, C. A.; Eisler, H. J.; Bawendi, M. G. Optical gain and stimulated emission in nanocrystal quantum dots. *Science* **2000**, *290*, 314−317.